IEEE Journal of Microwaves

Received 3 June 2024; revised 19 August 2024 and 25 November 2024; accepted 2 December 2024. Date of publication 23 December 2024; date of current version 9 January 2025.

Digital Object Identifier 10.1109/JMW.2024.3512368

Digital Pre-Distortion to Reduce Ringing in a Pulse Sharpening Non-Linear Transmission Line

STEPHEN PANCRAZIO, TYLER KELLEY, SAM WAGNER, NHAT TRAN, ABABIL HOSSAIN, AND ANH-VU PHAM (Fellow, IEEE)

(Regular Paper)

Department of Electrical and Computer Engineering, University of California Davis, Davis, CA 95616 USA

CORRESPONDING AUTHOR: Tyler Kelley (e-mail: tfkelley@ucdavis.edu).

This work was supported by the Department of the Navy, Office of Naval Research under Award N00014-22-1-2167.

ABSTRACT In this paper, we present the development of a digital pre-distortion (DPD) algorithm to reduce ringing in a UWB transmitter with a non-linear transmission line. Notably, this DPD is applied to a lower frequency bandwidth input pulse, translated to a much larger bandwidth output pulse where the ringing is reduced at the output pulse. A software-defined transmitter using an arbitrary waveform generator with 2.5 GHz of bandwidth implements the developed DPD algorithm. The non-linear transmission line sharpens the pulse to extend its bandwidth to 8 GHz. The DPD algorithm is developed using a look-up table of pulses characterized from the pulse sharpening system. The DPD algorithm reduces measured peak ringing in the output of the non-linear transmission line from −15.24 dB to −20.18 dB and RMS ringing from −26.4 dB to −30.5 dB.

INDEX TERMS Non-linear transmission line, digital pre-distortion, UWB pulse, software-defined transmitter.

I. INTRODUCTION

Ultrawideband (UWB) radar systems such as ground penetrating radar (GPR), through-wall radar, and short-range impulse radar are widely used in many applications. A finer resolution is desirable for more precise target sensing in each of these applications. To achieve fine resolutions, designers will aim to expand the bandwidth of the transmitted UWB pulse [1], [2]. In [3], types of pulse generators for UWB systems with high bandwidth pulses are detailed. Among the various types of pulse generators, transmitters have been created with step recovery diodes, avalanche transistors, and FETs. Also, [3] demonstrates that non-linear electrical transmission lines (NLETSs) can be leveraged for enhanced pulse propagation. Further, a Non-Linear Capacitive Transmission Line (NLCTL) uses an LC ladder network of lumped varactors and inductors for rise time compression. In this case, the varactors enact a non-linearity that increases the pulse's bandwidth. Thus, a non-linear transmission line (NLTL) is commonly employed to sharpen the UWB pulses in the time domain, expanding the pulse bandwidth [4], [5], [6], [7], [8], [9]. However, with the sharpened pulse, significant solitons and distortion will follow the pulse envelope [10], [11]. Fig. 1 illustrates an NLTL's effect, showing the component's normalized input and output pulse shapes.

While pulse bandwidth is essential for imaging, minimizing pulse ringing is also vital. Ringing can be defined as subsequent waveforms, like solitons or energy following the desired pulse envelope [12], [13], [14]. Due to ringing, received waveforms in UWB systems may contain additional returns to those from detected targets [15]. These additional returns can create false targets and degrade image quality, which must be diminished to improve pulse quality for radar systems.

Previous approaches have been implemented to reduce ringing in UWB pulses. Hardware modifications are a common method to reduce ringing such as those made to the amplifiers and antennas in [16], [17]. Specifically, antenna

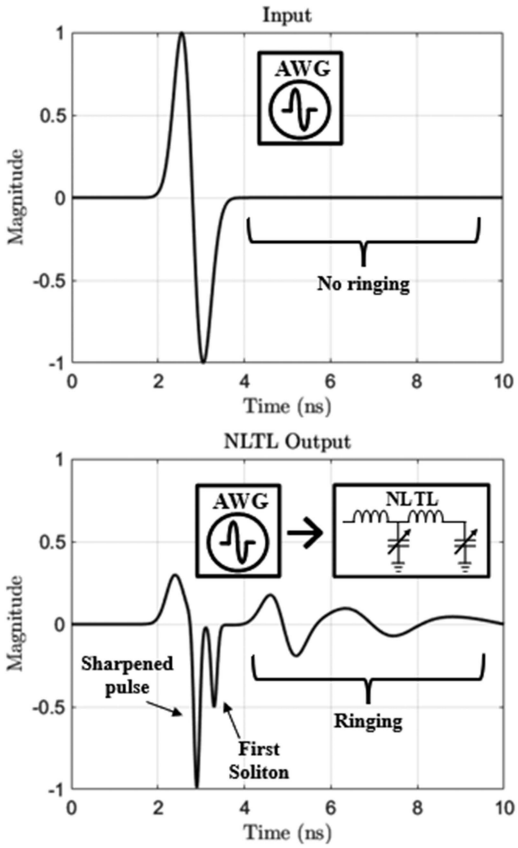

FIGURE 1. Normalized ideal input pulse and output sharpened pulse that has distortion caused by NLTL.

designs using a resistively loaded vee dipole antenna can be a hardware design effective in reducing late time ringing [16]. Other strategies leverage direct digital synthesis to reduce pulse ringing. These methods rely on a software-defined transmitter with an arbitrary waveform generator (AWG) where the waveform may be readily programmed by the user [18], [19], [20], [21], [22]. Using an AWG, digital pre-distortion (DPD) may be applied to transmitted UWB pulses to shape the input waveform and decrease ringing in the received pulse. [23] uses an iterative optimization to continually change the input pulse in segments in the time domain such that the peak output pulse ringing drops 7.9 dB. [24] also adds a Weiner filter to this iterative optimization to reconstruct the intended pulse shape while dropping the RMS ringing by 11.27 dB. Notably, [23] and [24] reduce ringing where the input and output pulse have the same frequency bandwidths.

These previously described DPD approaches have focused on compensating for in-band ripples in a linear system where the input and output signals have the same frequency. Additionally, these techniques have relied on a signal generator with a bandwidth equal to or larger than the output signal. Digital pre-distortion for a low-bandwidth signal translated to a high-frequency bandwidth using a non-linear transmission line has yet to be addressed for UWB applications. Furthermore, the arbitrary waveform generator usually has limited bandwidth in these systems and relies on a non-linear transmission to increase the bandwidth of the output signal. In a non-linear system with a higher output bandwidth, the compensation methodology may no longer be direct, as the output ringing may also have a higher frequency bandwidth than the input compensation. In addition, the lower frequency compensation will undergo a non-linear translation that must be accounted for to compensate for the output ringing accurately.

In this paper, we present a novel digital pre-distortion algorithm that reduces pulse ringing in the time domain from a non-linear transmission line. While the 20-dB pulse bandwidth out of the NLTL (an NLCTL design) is approximately 8 GHz, the DPD is programmed through an AWG limited to 2.5 GHz of bandwidth at the input. Thus, a lookup table-based strategy is employed for this digital pre-distortion to account for the system's nonlinearity. This algorithm works in a loop to continuously reduce the maximum ringing in the output waveform. Applying this DPD, the RMS ringing decreases by 4.94 dB while the peak ringing decreases by 4.1 dB for the NLTL output pulse. To the best of our knowledge, this is the first DPD algorithm used to compensate for a pulse sharpening component using a signal generator with a much lower bandwidth than that of the output pulse.

II. WHY IS DPD DIFFERENT FOR A NON-LINEAR COMPONENT?

The two main reasons why conventional DPD, seen in [23], [24], cannot be applied are the system's non-linearity and the increased frequency bandwidth of input to output pulse. Typically, DPD would consider in-band variations for the amplitude and phase of the system transfer function and apply direct compensation to negate them. However, the pulse sharpening of the NLTL expands the bandwidth of the output pulse compared to that of the AWG. This, in turn, changes the pulse's characteristic shape and introduces higher frequency ringing to the output. We can better characterize this issue in the simulation where the input pulse to the NLTL is set to the fastest possible pulse out of the AWG.

In this system, the main contributor of non-linearity is the NLTL. Due to the implementation of varactor diodes along a transmission line, portions of the pulse with higher voltage amplitudes travel faster than those with lower amplitudes. This can be represented by the group velocity equation, defined in [25], as in (1) below:

$$v_n = \frac{1}{\sqrt{L_n\, C_n(V)}} \tag{1}$$

where $C_n(V)$ represents a non-linear relationship between varactor capacitance and the pulse amplitude, L_n represents the inductance of a given transmission line segment, and v_n represents the group velocity. Therefore, by increasing the voltage of the pulse, we are effectively reducing the rise time of the pulse. Additionally, with this non-linear relationship, the non-uniformity in the group velocity will result in a shockwave phenomenon where several pulses follow the main pulse. The following pulses can form a secondary pulse,

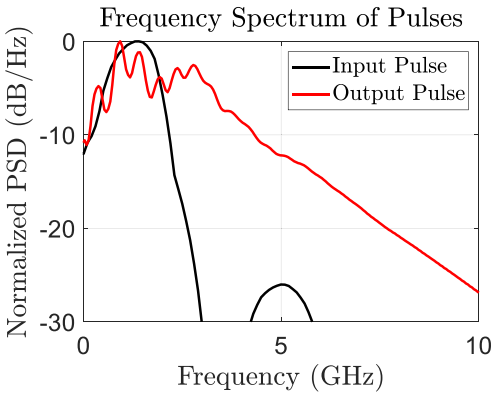

FIGURE 2. **Frequency spectrum of input versus output pulse for designed NLTL.**

not part of the main pulse, known as solitons. These solitons add to the ringing for the propagated UWB pulse. For a given NLTL, the soliton pulse width is determined by the maximum capacitance of the varactor used in addition to the inductance per segment of the transmission line. In literature, soliton amplitudes have been shown to constitute significant ringing in output waveforms from NLTLs, up to 60% for that of the main pulse depending on design [23]. As compared to other components in a UWB system, including amplifiers and antennas, the non-linearity effect of the NLTL will relatively dominate the pulse shape and ringing.

While the NLTL is the dominant source of non-linearity in the chain, additional non-linearity arises from the amplifiers used in the signal chain. As with most amplifiers propagating wideband signals, there are further non-linearities present in the harmonics generated from the frequency content of the UWB input signal. Additionally, temperature variations of the amplifier over time can alter its electrical characteristics, leading to non-linearities in the output signal. Moreover, when using a GaAs amplifier in the chain, there may be gate lag due to a delay in the current response when the voltage pulse is initially applied to the gate. This gate lag manifests in the output pulse as a slower rise and fall compared to the input. Overall, while the effects of the amplifiers are significant, the NLTL remains the primary cause of the output pulse's non-linearity, as solitons will dominate ringing in the time domain.

Fig. 2 displays the input versus output pulse normalized frequency spectrum for the NLTL. The fastest possible input pulse spectrum was originally measured directly from the AWG. That input pulse was then imported to the NLTL design in Advanced Design System (ADS). The resulting output pulse is generated from a time-domain simulation. As evident from the plot, the output pulse of the AWG has a 20-dB bandwidth only up to 2.5 GHz, while the output pulse of the NLTL covers up to 8 GHz. The ringing from solitons in the output pulse tends to be similar to the main output pulse in frequency content due to the designed Bragg frequency of the NLTL [26]. As such, the AWG cannot directly compensate for the ringing in the output signal because the AWG cannot generate content at the frequency of the follower solitons. To properly compensate for the ringing, the AWG must generate compensation at a lower bandwidth that is then upconverted by the NLTL.

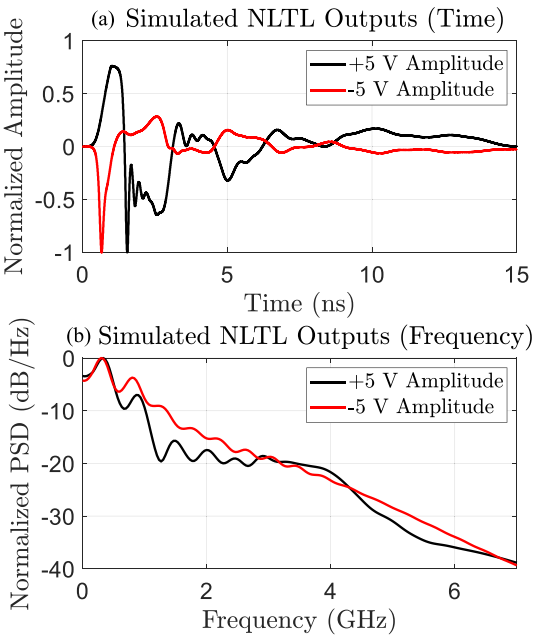

FIGURE 3. **Output pulses from the NLTL for Gaussian pulses with amplitudes of +5 V and -5V in the (a) time and (b) frequency domains.**

Furthermore, the effect of the non-linearity on a given input is not necessarily scalable. Due to the varactor diodes in the NLTL, a pulse with a positive polarity will result in a fundamentally different output pulse waveform shape than one with a negative polarity at the same amplitude. An example of this phenomenon is shown in Fig. 3, where the output waveforms of the NLTL for two Gaussian pulse inputs (with 20-dB bandwidths of 2.5 GHz) amplitudes of +/-5 V have fundamentally different shapes.

In Fig. 3(a), the time domain shapes of the respective output pulses differ significantly due to polarity. The negative output pulse is subject to sharpening, resulting in a thinner output pulse, while the positive shows a differential output pulse with no sharpening. Furthermore, before normalization, the peak amplitude of the output for the −5 V input is −7.52 V, a 50.4% increase from the input amplitude, while the peak amplitude of the +5 V input is only −3.2 V, a 36% decrease from the input amplitude. The pulse flattening effect is further displayed in Fig. 3(b) through the bandwidth expansion of the output pulse. Furthermore, ringing following each of these pulses is different in frequency and amplitude profiles. These factors must be considered for DPD, as the changes to the output pulse will depend on the input compensation's size and polarity. Thus, a DPD algorithm using a look-up table can map the resulting outputs for all potential input compensation to account for the system's nonlinearity.

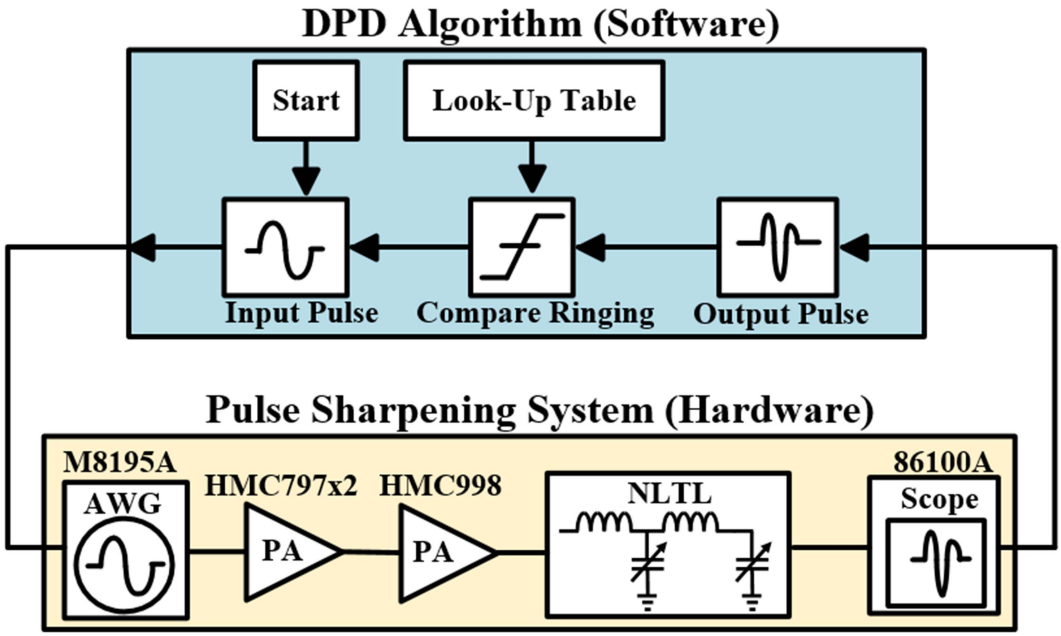

FIGURE 4. The DPD algorithm and system hardware, including amplifiers and NLTL.

III. METHODOLOGY

Fig. 4 shows the system, including both software and hardware. The proposed DPD algorithm is displayed in the blue box. The DPD algorithm is implemented in software through MATLAB. The hardware shown in the beige box includes the arbitrary waveform generator, amplifiers, non-linear transmission line, and oscilloscope. The DPD methodology can be described in six steps:

- *Step 1:* Determine width and shape of the starting input pulse and program it to the AWG.
- *Step 2:* Generate a low-frequency pulse from the AWG, which is then sharpened by the non-linear transmission line. Quantify the peak ringing present in the output waveform of the NLTL.
- *Step 3:* Generate a set of pulses from the AWG to form a lookup table. The peak ringing will be the upper amplitude limit of the input pulses. The input and output pulses are saved in a look-up table.
- *Step 4:* Compare waveforms in the look-up table to peak ringing in the measured output waveform. Choose a pulse from the lookup table that negates peak ringing and add it to the new input pulse.
- *Step 5:* After compensation, read the new output pulse and quantify its maximum ringing.
- *Step 6:* Repeat Steps 4 and 5 until the peak ringing of the output waveform no longer decreases.

A. STEP 1: PULSE DEFINITION

Initially, the starting pulse in the time domain, $X_0(t)$, is defined in software. For this system, a differential pulse, the derivative of a Gaussian pulse, was chosen as the pulse shape. Based on simulation results, the shape was chosen so that it would maximize the input voltage drive to the NLTL compared to a Gaussian pulse. The starting differential pulse in the time (t) domain, $X_0(t)$, is defined using σ in (2) as seen in [27]:

$$X_0(t) = -\frac{t}{\sigma^2} e^{-\frac{1}{2}\left(\frac{t}{\sigma}\right)^2} \tag{2}$$

The variable σ controls the pulse width in the time domain as a larger value will mean a wider pulse. In the case of this system, we use the maximum capabilities of the AWG which has a 20-dB bandwidth of 2.5 GHz and a σ of 180 ps for a differential pulse.

B. STEP 2: STARTING PULSE PROPAGATION

The ADS7-V2EBZ data acquisition and the AD9162 digital-to-analog converter (DAC) boards form an arbitrary waveform generator (AWG) used to generate the starting input pulse, $X_0(t)$. The pulse signal then propagates through the pulse sharpening system, including the HMC797 power amplifiers, HMC998 power amplifier, non-linear transmission line, and PE7318-20 attenuator. The first received output pulse, $Y_0(t)$, is measured from the 86100A oscilloscope. Once accessible in software, the input and output pulses are aligned in time. Table 1 below lists the components used and their bandwidth specifications.

The pulses are aligned by artificially shifting the output pulse until it reaches a maximum cross-correlation with the input pulse, as used in [22]. After t_0, the output pulse should be flat where non-zero content is considered ringing. The final measured point in the waveform is referred to as t_{last}.

Importantly, the input waveform is generated from a lower-speed AWG with a 5 GHz DAC sampling rate. A lower sampling rate for signal generation inherently limits where

TABLE 1. Hardware Used for Pulse Sharpening System

Part	Component Name	Bandwidth
Arbitrary Waveform Generator	Analog Devices ADS7-V2EBZ + AD9162 boards	DC-2.5 GHz
Transmitter Amplification	2x Analog Devices HMC797 PAs and 1x HMC998 PA	DC-22 GHz
Non-Linear Transmission Line	48 x Skyworks SMV2019	DC-8 GHz
Attenuator	Pasternack PE7318-20	DC-18 GHz
Receiver	Agilent 86100A Sampling Oscilloscope	DC-50 GHz

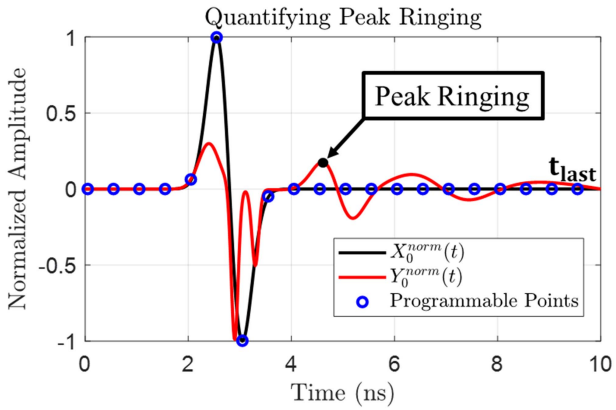

FIGURE 5. Measured input pulse, output pulse, and controllable points. The maximum ringing point is labeled between t_0 and t_{last}.

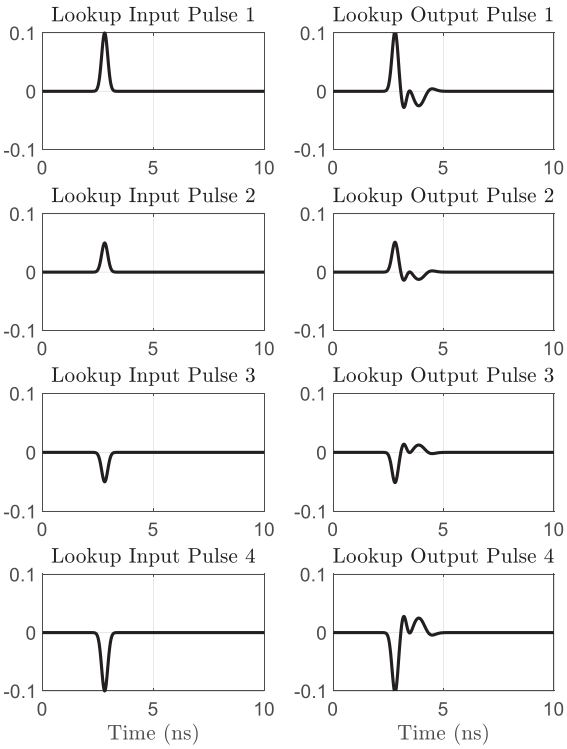

FIGURE 6. Example illustration of a lookup table with four input and output pulses stored and a peak ringing ratio of 0.1.

DPD compensation may be applied. There is only a specific set of programmable points in the time domain where the input pulse can be directly modified. For brevity, we refer to points where the AWG may modify the input pulse directly as programmable points. Considering only time domain points that align with programmable points of the input, we define the peak ringing point in the output waveform. The synchronized normalized input pulse, $X_0^{norm}(t)$, and output pulse, $Y_0^{norm}(t)$, are illustrated in Fig. 5. Additionally, the programmable points of the AWG are plotted over the input and the maximum ringing point is labeled on the output.

We normalize the peak ringing value to the maximum pulse amplitude of as seen in (3) below as seen in [23]:

$$Peak\ Ringing\ Ratio = \left(\frac{Peak\ Ringing}{Peak\ Pulse\ Amplitude}\right) \tag{3}$$

C. STEP 3: FORMING THE LOOKUP TABLE

After the peak ringing is determined, the lookup table can be constructed. The input pulses used for the lookup table consist entirely of Gaussian pulses generated by the AWG. In this case, the AWG can produce Gaussian pulses with a 20-dB bandwidth of 2.5 GHz due to its 5 GHz DAC rate. A Gaussian pulse, $X_G(t)$, is defined in the time domain (t) using σ in (4):

$$X_G(t) = e^{-\frac{1}{2}\left(\frac{t}{\sigma}\right)^2} \tag{4}$$

All input pulses used for the lookup table are Gaussian pulses with $\sigma = 137$ ps correlating to a 2.5 GHz 20-dB bandwidth. Again, this pulse shape is determined because it is the fastest available pulse out of the AWG. As such, the input pulses used to construct the lookup table are only adjusted by their relative amplitudes. The maximum amplitude of any input pulses in the look-up table is set based on the calculated peak ringing ratio in (3). For example, if the peak ringing ratio is 0.1 then the largest input pulse used in the lookup table will be 10% of the full amplitude of the initial input pulse, $X_0(t)$. The maximum scale determines the first pulse in the lookup table. Conversely, an inverted Gaussian pulse with that same amplitude determines the last pulse for the lookup table. In the current example, that would mean the amplitude scalar for the last pulse would be -0.1.

To determine the size of the lookup table, the user sets the total number of pulses. The remaining pulse amplitudes are set such that from either polarity, the lookup table amplitudes scale linearly to zero. For example, if the user chose four pulses to make up the lookup table, the lookup table amplitude scalars would be 0.1, 0.05, −0.05, and −0.1. Each input pulse defined in the lookup table is then propagated through the pulse sharpening system. Each resulting output waveform is read by the oscilloscope and stored with its corresponding input in the lookup table. An example of a lookup table with four input and output pulses using a peak ringing ratio of 0.1 is illustrated in Fig. 6.

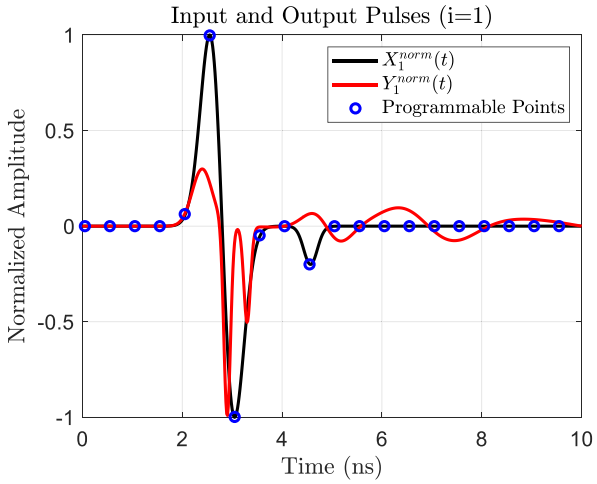

FIGURE 7. New input pulse, new output pulse, and controllable points for i = 1.

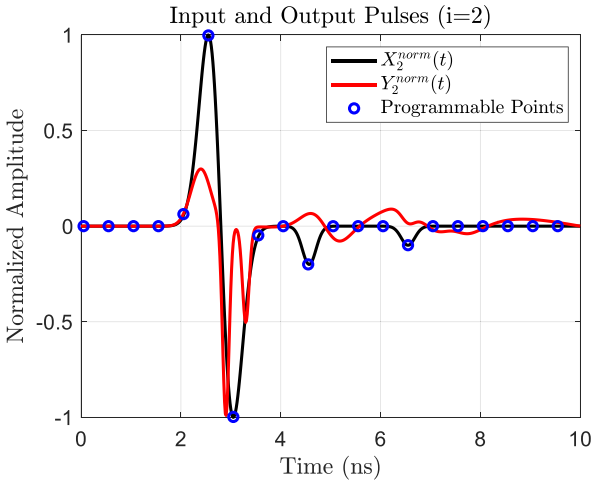

FIGURE 8. New input pulse, new output pulse, and controllable points for i = 2.

D. STEP 4: FORMING THE NEW INPUT PULSE

To form the new input pulse, the optimal compensation from the lookup table must be selected. In software, each pulse stored in the lookup table is shifted to be aligned with the peak ringing in the output. Each output pulse from the lookup table is individually added at that instance of peak ringing to the measured output pulse. The ringing for each scenario after pulse addition is recalculated, and the ringing is quantified. This procedure estimates the output pulse if compensation from the lookup table was added at that point. Then, the pulse from the lookup table resulting in the lowest peak ringing in the compensated pulse is chosen. The corresponding input pulse from the lookup table is added to the previous input to form the new input pulse, $X_1(t)$.

E. STEP 5: READ THE NEW OUTPUT PULSE

Once the new input pulse is determined in software, the AWG once again synthesizes the newly pre-distorted input pulse, $X_1(t)$. Once formed by the AWG, the pulse passes through the pulse sharpening system, and the new output pulse with a larger bandwidth, $Y_1(t)$, is read by the oscilloscope. The ringing portion of the waveform of the new output pulse is found, and its new maximum ringing value is quantified. The peak ringing present in $Y_1(t)$ should have decreased compared to $Y_0(t)$. Fig. 7 displays normalized plots of $X_1^{norm}(t)$ and $Y_1^{norm}(t)$.

F. STEP 6: REPEAT THE PROCESS

Following the same process as described in Steps 4 and 5 above, a new input pulse, $X_i(t)$, for an iteration, i, is formed through adjustments from the lookup table and subsequently propagated through the pulse sharpening system. The subsequent output pulse, $Y_i(t)$, is then read at the oscilloscope. These steps are repeated until the maximum ringing is no longer decreasing. This process is shown for $i = 2$ in Fig. 8 below.

If the peak ringing increases at any point, the algorithm will automatically return to the input with minimum ringing. At this point, the algorithm ends and the final output with reduced ringing can be quantified.

G. METRICS FOR DPD

To determine the effectiveness of the DPD algorithm, we use two metrics: RMS ringing and peak ringing. The RMS ringing is calculated using the time domain waveform following the pulse envelope [23]. From the start of the ringing, t_0, to its final point, t_{last}, the RMS value of the normalized output waveform, $Y^{norm}(t)$, in the dB scale for a number of points N is found in (5):

$$RMS\ Ringing = 20\log_{10}\left(\sqrt{\frac{\sum_{t_0}^{t_{last}}(Y^{norm}(t))^2}{N}}\right) \quad (5)$$

Peak ringing may be defined as the maximum value in the residual ringing plot from the output voltage waveform in the dB scale. Generally, a value below −20 dB is desirable for radar applications [15].

IV. SIMULATION RESULTS

The NLTL was designed in an Advanced Design Systems (ADS) simulation environment while the algorithm is performed in MATLAB. In ADS, a time domain waveform can be programmed at the input of the NLTL. A realistic UWB pulse representing an amplified differential pulse with a 14 Vpp is defined in MATLAB and sent to ADS. The pulse bank consists of ten Gaussian pulses scaled linearly using a peak ringing ratio of 0.126. The initial pulse output is generated in ADS. The compensation is applied in MATLAB, and the new pre-distorted input is exported to ADS. The process is repeated until peak ringing no longer decreases. In the simulation, the algorithm finishes after 11 iterations. An annotated picture of the ADS environment is included for clarity below in Fig. 9.

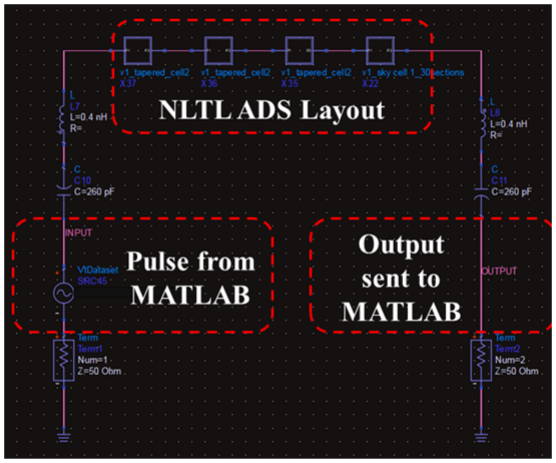

FIGURE 9. ADS implementation of the NLTL line. The input pulse is formed and imported from MATLAB to ADS. After simulating the pulse in ADS, the output pulse is exported to MATLAB.

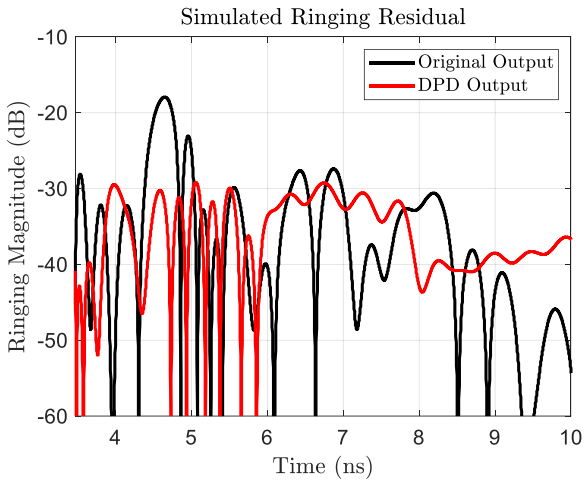

FIGURE 11. Residual ringing waveforms with and without DPD in simulation.

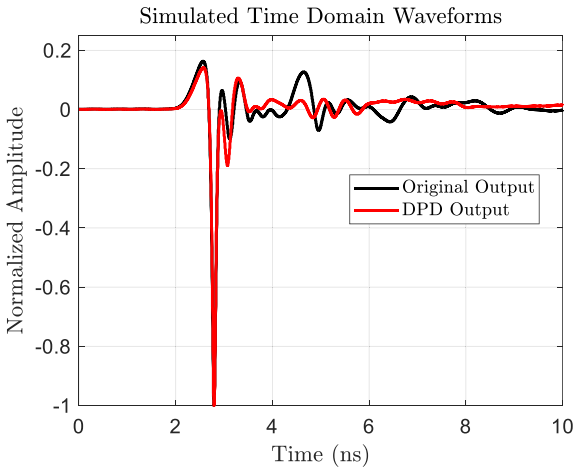

FIGURE 10. Time domain waveforms with and without DPD in simulation.

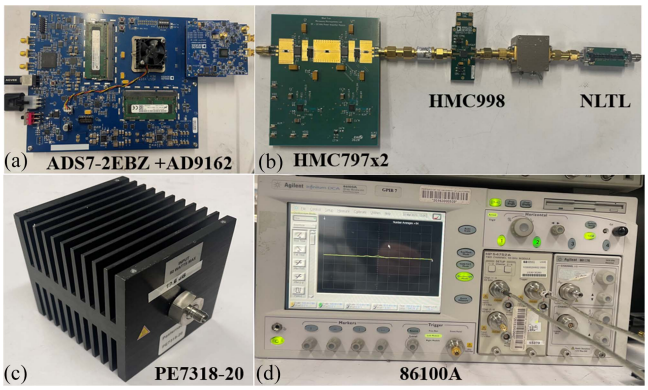

FIGURE 12. Pictures of the (a) data acquisition and DAC boards that make up the AWG, (b) amplifiers and non-linear transmission line under test, (c) attenuator used after NLTL, and (d) oscilloscope used to read waveform.

In Fig. 10, the simulated normalized output waveforms with and without DPD are shown in the time domain from 0 to 10 ns. Using the DPD, we find that the ringing after the first soliton is significantly flattened. This effect is specifically seen for the oscillation at 4.3 ns in the original output waveform. The peak ringing ratio drops nearly 75% from a normalized value of 0.126 to 0.034. In all, the ringing following the pulse envelope only has minor oscillations remaining after DPD.

This drop in ringing is captured in Fig. 11, which displays the residual ringing plots with and without DPD. The ringing is plotted from 3.5 to 10 ns. Over this range, the peak ringing reduced from −17.94 dB to −30 dB for a 12.06 dB reduction. The ringing at every point is kept below −30 dB in the output with DPD. While there are several individual points where ringing worsens slightly, these degradations are negligible as the value at these points is already close to zero. Moreover, the RMS ringing decreased from −26.65 dB to −30.7 dB in simulation with DPD.

V. MEASUREMENT RESULTS

Fig. 12 shows pictures of the pulse sharpening system hardware for our experiment. In Fig. 12(a), the Analog Devices ADS7-V2EBZ data acquisition board and AD9162 digital-to-analog converter (DAC) boards forming the AWG are shown. The pulse produced from the AWG has a peak-to-peak amplitude of 0.4 V and a 20-dB bandwidth of 2.5 GHz. In Fig. 12(b), the first amplifier board contains a cascade of two DC-22 GHz HMC797 power amplifiers with active bias control. After DC-22 GHz amplifier module, another DC-22 GHz HMC998 amplifier is used to drive the NLTL. With this amplification chain, the pulse input to the NLTL has a voltage swing of 14 V peak-to-peak. Next, the pulse reaches a 50-stage NLTL loaded with Skyworks SMV2019 varactors. The NLTL is designed to produce a pulse with an 8 GHz 20-dB bandwidth. Lastly, Fig. 12(c) shows the Pasternack PE7318-20 attenuator providing 19.6 dB of attenuation up to 18 GHZ. The attenuator is a necessary component to protect

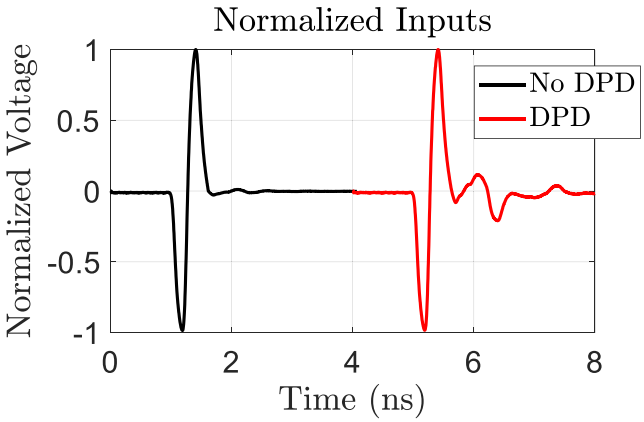

FIGURE 13. Measured input pulse waveforms with and without DPD.

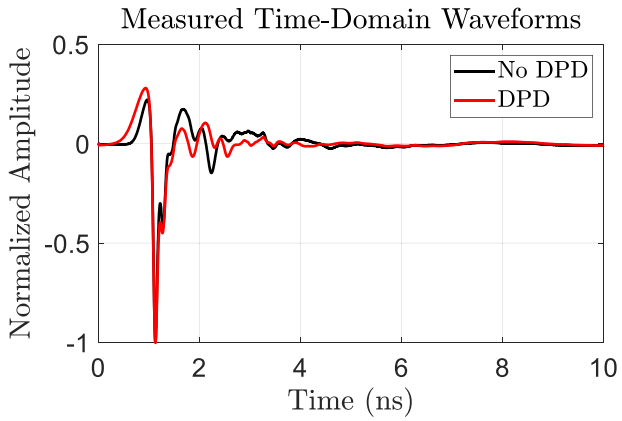

FIGURE 14. Time domain waveforms with and without DPD in measurement.

the oscilloscope. Next, the Agilent 86100A 50 GHz sampling oscilloscope used to read the output pulse is displayed Fig. 12(d).

The DPD algorithm is run entirely on MATLAB for this system. In measurements, the algorithm loop ran 13 times before reaching the minimum peak ringing value. Fig. 12 shows the normalized input pulses with and without DPD. The waveform without DPD approximates a differential input pulse, while the pulse with DPD contains several oscillations following the pulse envelope. As expected, each of these oscillations portrays a different sized Gaussian pulse that was added as compensation.

In Fig. 14, the measured normalized output waveforms with and without DPD are shown in the time domain from 0 to 8 ns. Peak ringing drops by nearly 43% from a normalized value of 0.172 to 0.098. The residual ringing plots from 0 ns to 10 ns are captured in Fig. 15. Over this range, the peak ringing decreased from −15.24 dB to −20.18 dB. The ringing at every point is kept below −20 dB after using DPD. Overall, the ringing for the waveform with DPD is significantly flattened compared to the waveform without DPD. The RMS ringing decreased from −26.4 dB to −30.5 dB in measurements through DPD. While the improvement in peak

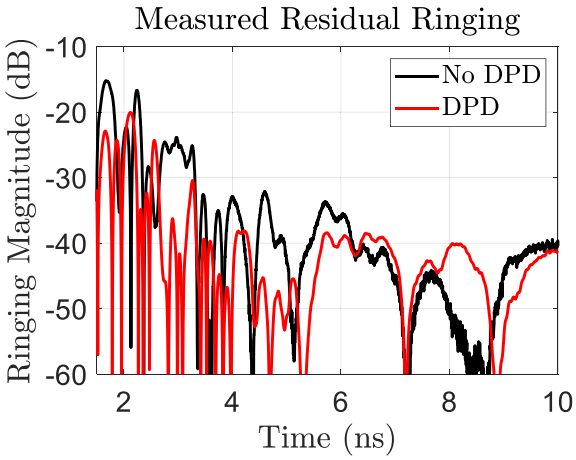

FIGURE 15. Residual ringing waveforms with and without DPD in measurement.

TABLE 2. Measured Performance Comparison With and Without DPD

	Peak Ringing	RMS Ringing
No DPD	-15.24 dB	-26.4 dB
DPD	-20.18 dB	-30.5 dB

TABLE 3. Ringing Performance Comparison to Other NLTL Transmitters

Ref.	Output 20-dB Bandwidth (GHz)	Design Type	Peak Soliton Ringing
[26]	4.4	Tapered	-20 dB
[28]	0.07	Hybrid	-4.44 dB
[29]	78	Tapered	-10.46 dB
[30]	100	Tapered	-6.74 dB
Our Design	8	Tapered	-20.18 dB

ringing reduction is slightly less than what was achieved in simulation, the simulated and measured RMS ringing results are quite similar comparatively.

The overall measured findings for the impact of this DPD algorithm on ringing are summarized in Table 2 below.

To better understand these results, we can compare the ringing performance with that described in [26], [28], [29], [30], which implement comparable NLTL designs. Table 3 below characterizes their design performance in terms of soliton size and how that translates to their respective peak ringing, based on a table previously reported in [26]. References [28], [29], [30] show distinctly higher peak ringing from the captured solitons compared to the output of this algorithm. Notably, [26] employs a distinct tapering strategy for soliton reduction, achieving a similar performance with a peak ringing of -20 dB. Consequently, this algorithm applies compensation that slightly exceeds the peak ringing in hardware specifically designed to reduce solitons. The potential application of this algorithm on that NLTL may further diminish soliton-based ringing.

VI. COSTS AND TRADEOFFS

There are an assorted number of tradeoffs to keep in mind when weighing the usefulness and practicality of the presented algorithm for the UWB transmitter. Among the concerns for potential complexity costs of the system are the algorithmic function itself and the AWG. The AWG is a complex hardware as compared to a simple pulse transmitter. However, the AWG makes DPD possible and generates pulses defined by software. The complexity cost of the algorithm will be heavily dependent on the amount of pulses used in the look up table as dictated by the user. As such, the user controls the complexity of the algorithm. The complexity and time needed for the algorithm increase linearly with each pulse added to the lookup table, as the same subtraction and ringing comparison must be computed for all pulses in every iteration. However, with additional waveforms, the final resolution of the DPD compensation will also increase linearly. With proper awareness of system speeds, the size of a lookup table can be properly set by the user for real-world applications. It is worth noting that once DPD is applied to a specific transmitting chain and input pulse, the algorithm does not need to be re-implemented, thereby reducing the complexity for future operation.

Regarding material costs, there are associated tradeoffs with implementing an NLTL for bandwidth expansion. System complexity inherently increases as the NLTL is another added element to the signal path. Further, the NLTL necessitates its own power supply that any implemented power distribution network must be able to source. There is additionally a financial cost to implementing the NLTL, as in-house fabrication plus assembly for the part costs approximately $500 for this specific design. However, that cost may be dropped significantly with increased production of the design in bulk. Further, the NLTL being used for frequency expansion can be a much cheaper and simpler option in comparison to alternatives such as a faster arbitrary waveform generator.

A hybrid or magnetic NLTL could be useful as the non-linearity would not only come from the physical properties of the varactor diodes but would also come from non-linear inductors utilizing ferromagnetic cores [31]. If this design were to be implemented with non-linear inductors, the design would have to be modified as the non-linearity would come from the current of the pulse, not the voltage amplitude. Potentially, this could lend itself to further pulse sharpening as compared to the current NLTL. While these other NLTL lines improve pulse sharpening, we implemented a more traditional NLCTL model for the sake of simplicity, size, and cost.

Adapted versions of this algorithm may also have value. As for being applied to different platforms, the core of this algorithm can flexibly be implemented in any other software that allows for storing arrays in a lookup table-based format. In a heterodyne mixer-based transmitter platform, this algorithm can be readily applied to reduce ringing due to frequency translation. In this context, it may be beneficial to incorporate a portion of the algorithm that considers the output frequency spectrum in addition to the time-domain compensation outlined in the paper. Overall, there are still opportunities to further expand the algorithm for broader applications beyond pulsed UWB time-domain corrections.

In all, there are certainly both time and complexity costs that come with the implementation of DPD. However, for designs of UWB systems where ringing must be minimized for either effective communication or imaging, DPD can be a preferable alternative due to its inherent flexibility. The implementation of the DPD algorithm does not have the same time and financial costs associated with it as the potential design of custom hardware to meet low ringing specifications such as that seen in [14], [15], and [25]. Additionally, due to the flexibility of the algorithm, the 4.94-dB reduction in peak pulse ringing achieved in this work can be potentially recreated for other systems through this algorithm. This DPD can be applied to any system signal chain to relieve constraints on hardware, saving both time and financial expenses of the design process.

VII. CONCLUSION

In this paper, we present a digital pre-distortion (DPD) algorithm used to reduce ringing in output pulse with a comparatively higher frequency bandwidth than that of the input pulse. The software-defined transmitter with an NLTL is leveraged to readily re-program the input waveform using a generated look-up table. The DPD reduces the peak ringing of the output waveform by 4.94 dB and RMS ringing by 4.1 dB. This DPD technique can be applied to compensate for other non-linearities in UWB systems. The flexibility to readily change the input waveform through use of direct digital synthesis could continue to be useful in future UWB transmitter designs. In future work, it would be worthwhile to optimize the algorithm to lessen the linearly scaling complexity of the lookup table implemented.

ACKNOWLEDGMENT

Any opinions, findings, and conclusions or recommendations expressed in this material are those of the author(s) and do not necessarily reflect the views of the Office of Naval Research.

REFERENCES

[1] J. Han and C. Nguyen, "Development of a tunable multiband UWB radar sensor and its applications to subsurface sensing," *IEEE Sensors J.*, vol. 7, no. 1, pp. 51–58, Jan. 2007.

[2] S. Wagner, S. Pancrazio, A. Hossain, and A.-V. Pham, "Experimental detection of buried sub-mm diameter wires using microwave ground-penetrating radar," in *Proc. IEEE USNC-URSI Radio Sci. Meeting (Joint AP-S Symp.)*, Singapore, 2021, pp. 37–38.

[3] K. Wu and M. Rahman, "Pulse generation and compression techniques for microwave electronics and ultrafast systems," *Electromagn. Sci.*, vol. 1, no. 1, Mar. 2023, Art. no. 0010131.

[4] J. M. Sanders, Y.-H. Lin, R. Ness, A. Kuthi, and M. Gundersen, "Pulse sharpening and soliton generation with nonlinear transmission lines for producing RF bursts," in *Proc. IEEE Int. Power Modulator High Voltage Conf.*, Atlanta, GA, USA, 2010, pp. 604–607.

[5] S. Ibuka, M. Ohnishi, T. Yamada, K. Yasuoka, S. Ishii, and K.-C. Ko, "Voltage amplification effect of nonlinear transmission lines for fast high voltage pulse generation," in *Proc. 11th IEEE Int. Pulsed Power Conf.*, 1997, vol. 2, pp. 1548–1553.

[6] J. D. C. Darling and P. W. Smith, "High-power pulsed RF extraction from nonlinear lumped element transmission lines," *IEEE Trans. Plasma Sci.*, vol. 36, no. 5, pp. 2598–2603, Oct. 2008.

[7] E. Afshari and A. Hajimiri, "Nonlinear transmission lines for pulse shaping in silicon," *IEEE J. Solid-State Circuits*, vol. 40, no. 3, pp. 744–752, Mar. 2005.

[8] F. Yu, K. G. Lyon, and E. C. Kan, "A low-power UWB-IR transmitter by tapered nonlinear transmission lines," *IEEE Microw. Wireless Compon. Lett.*, vol. 22, no. 12, pp. 618–620, Dec. 2012.

[9] L. P. Silva Neto, J. O. Rossi, and J. J. Barroso, "Pulse sharpening and RF generation using nonlinear transmission lines," in *Proc. SBMO/IEEE MTT-S Int. Microw. Optoelectron. Conf.*, Porto de Galinhas, Brazil, 2015, pp. 1–6.

[10] A. J. Fairbanks, A. M. Darr, and A. L. Garner, "A review of nonlinear transmission line system design," *IEEE Access*, vol. 8, pp. 148606–148621, 2020.

[11] M. Rahman and K. Wu, "A nonlinear transmission line technique for generating efficient and low-ringing picosecond pulses for ultrabroadband and ultrafast systems," *IEEE Trans. Instrum. Meas.*, vol. 71, 2022, Art. no. 2005511.

[12] Y. Jin, J. Chen, B. Liang, D. Yang, M. Xing, and L. Liu, "First demonstration of using signal processing approach to suppress signal ringing in impulse UWB through-wall radar," *IEEE Geosci. Remote Sens. Lett.*, vol. 19, 2022, Art. no. 3505505.

[13] S. Wagner and A.-V. Pham, "Structural effect on image quality degradation in ground-penetrating radar array," in *Proc. IEEE Int. Symp. Antennas Propag. USNC-URSI Radio Sci. Meeting*, 2019, pp. 1631–1632.

[14] M. U. Rahman, A. Haider, and M. Naghshvarianjahromi, "A systematic methodology for the time-domain ringing reduction in UWB band-notched antennas," *IEEE Antennas Wireless Propag. Lett.*, vol. 19, no. 3, pp. 482–486, Mar. 2020.

[15] S. Wagner, A. Hossain, S. Pancrazio, and A. Pham, "System-based specifications for better design of ground-penetrating radar antennas," *IET Microw., Antennas, Propag. J.*, vol. 17, pp. 1–16, 2023.

[16] S. Wagner and A.-V. Pham, "The ultrawideband elliptical resistively loaded vee dipole," *IEEE Trans. Antennas Propag.*, vol. 68, no. 4, pp. 2523–2530, Apr. 2020.

[17] X. Wang et al., "Impulse based range-gated UWB wireless transceiver IC in 90nm CMOS for medical sensing applications and communications," in *Proc. IEEE Int. Conf. Ultra-Wideband*, 2009, pp. 194–199.

[18] T. Norimatsu et al., "A UWB-IR transmitter with digitally controlled pulse generator," *IEEE J. Solid-State Circuits*, vol. 42, no. 6, pp. 1300–1309, Jun. 2007.

[19] I. V. Strelnikov, I. V. Ryabov, and E. S. Klyuzhev, "Direct digital synthesizer of phase-manipulated signals, based on the direct digital synthesis method," in *Proc. IEEE Syst. Signal Synchronization, Generating Process. Telecommun.*, 2020, pp. 1–3.

[20] P. Nilsson, J. F. M. Gerrits, and J. Yuan, "A low complexity DDS IC for FM-UWB applications," in *Proc. IEEE 16th IST Mobile Wireless Commun. Summit*, 2007, pp. 1–5.

[21] S. Pancrazio, S. Wagner, A. Hossain, T. Kelley, N. Tran, and A.-V. Pham, "0.35-11 GHz UWB radar system with software-defined transmitter and receiver," *IEEE Trans. Geosci. Remote Sens.*, submitted for publication.

[22] E. S. Eide and J. F. Hjelmstad, "A multi antenna ultra wideband ground penetrating radar system using arbitrary waveforms," in *Proc. IEEE Int. Geosci. Remote Symp.*, 1999, vol. 3, pp. 1746–1748.

[23] S. Pancrazio et al., "Digital pre-distortion to reduce ringing in ultrawideband radar systems," *IEEE Trans. Radar Syst.*, vol. 1, pp. 205–211, 2023.

[24] S. Pancrazio, P. Nguyen, S. Wagner, A. Hossain, and A.-V. Pham, "Digital pre-distortion to correct UWB pulses in a boresight test," in *Proc. IEEE Int. Symp. Antennas Propag. USNC-URSI Radio Sci. Meeting*, 2021, pp. 525–526.

[25] M. Rahman and K. Wu, "A nonlinear transmission approach to compressing rise and fall time in picosecond pulse generation," *IEEE Trans. Instrum. Meas.*, vol. 70, 2021, Art. no. 2004013.

[26] T. Kelley, S. Pancrazio, P. Emani, N. Tran, and A.-V. Pham, "A nonlinear transmission line with secondary soliton decimation," in *Proc. IEEE 20th Eur. Radar Conf.*, Berlin, Germany, 2023, pp. 452–455.

[27] H. M. Jol, *Ground Penetrating Radar: Theory and Applications*. Amsterdam, The Netherlands: Elsevier Science, 2009.

[28] N. S. Kuek, A. C. Liew, E. Schamiloglu, and J. O. Rossi, "Circuit modeling of nonlinear lumped element transmission lines including hybrid lines," *IEEE Trans. Plasma Sci.*, vol. 40, no. 10, pp. 2523–2534, Oct. 2012.

[29] M. G. Case, "Nonlinear transmission lines for picosecond pulse, impulse and millimeter-wave harmonic generation," Ph.D. dissertation, Dept. Electr. Comput. Eng., Univ. California, Santa Barbara, CA, USA, 1993.

[30] P. Indirayanti, W. Volkaerts, P. Reynaert, and W. Dehaene, "Picosecond pulse generation with nonlinear transmission lines in 90-nm CMOS for mm-wave imaging applications," in *Proc. 19th IEEE Int. Conf. Electron., Circuits, Syst.*, 2012, pp. 885–888.

[31] M. Rahman and K. Wu, "Theory and practice of multidimensional non-linear transmission line," in *Proc. IEEE MTT-S Int. Wireless Symp.*, Nanjing, China, 2021, pp. 1–3.